LAWRENCE
LIVERMORE
NATIONAL
LABORATORY

UCRL-CONF-216862

Different precursor populations revealed by microscopic studies of bulk damage in KDP and DKDP crystals

P. DeMange, R. A. Negres, H. B. Radousky, S. G. Demos

November 4, 2005

Boulder Damage Symposium
Boulder, CO, United States
September 19, 2005 through September 21, 2005

Different precursor populations revealed by microscopic studies of bulk damage in KDP and DKDP crystals

P. DeMange, R. A. Negres, H. B. Radousky, and S. G. Demos

Lawrence Livermore National Laboratory, 7000 East Avenue, Livermore, California 94551

ABSTRACT

We present experimental results aiming to reveal the relationship between damage initiating defect populations in KDP and DKDP crystals under irradiation at different wavelengths. Our results indicate that there is more than one type of defects leading to damage initiation, each defect acting as damage initiators over a different wavelength range. Results showing disparities in the morphology of damage sites from exposure at different wavelengths provides additional evidence for the presence of multiple types of defects responsible for damage initiation.

1. INTRODUCTION

With the construction of a new generation of large-aperture laser systems underway, understanding the fundamentals of laser-induced damage initiation mechanisms may offer the avenue to solve this problem. Potassium dihydrogen phosphate (KH_2PO_4 or KDP) and its deuterated analog ($KD_XH_{2-X}PO_4$ or DKDP) are currently the only nonlinear materials suitable as Pockel cells and frequency converters. Experimental efforts to determine the mechanisms of localized bulk damage initiation have provided important results that have helped to refine working theories. However, the makeup and types of the damage precursors is still unknown. Understanding the different type of defects leading to damage initiation at each operational frequency is a critical component to identifying their nature.

In this work, we investigate the different types of bulk defects that lead to damage initiation at different wavelengths by analyzing the damage behavior under exposure to 1064, 532, and 355 nm. Our results indicate the presence of two non-overlapping defect populations responsible for damage over different wavelength ranges. We also observe the damage site morphology at each wavelength under high resolution. Disparities in damage site features provide supporting evidence to suggest multiple defect types.

2. EXPERIMENTAL APPROACH

Figure 1 shows an illustration of the damage testing experimental setup. The damage testing is performed using a pulsed Nd:YAG laser at the fundamental (at 1064 nm), second, and third harmonics. High reflectivity mirrors selective to each harmonic are used to separate each harmonic of the output beam. The energy of each harmonic beam is controlled using a waveplate and polarizer combination. The three harmonic beams are then aligned to co-propagate and focused by a cylindrical lens (f = 200 mm) to the bulk of the material. Galilean telescopes are placed in each harmonic beam path to 1) decrease the diameter of each beam to 3 mm in order to use minimal material during testing and 2) correct for dispersion of the lens in order to have focus of each beam to the same place (centered within the sample bulk). The beam spatial profiles are measured using a 0.25 by 0.25 inch^2 CCD camera with a pixel resolution of ~ 5 μm. The beams focus to a $1/e^2$ height of 3 mm and widths of 90 μm, 60 μm, and 40 μm for 1064, 532, and 355 nm, respectively.

A microscope system is used to image the damaged volume through the side of the sample to determine the resulting damage pinpoint density (PPD) and size distribution of the damage sites. Assessment of the PPD is performed using % 2 magnification microscope objective followed by % 5 magnification lens which provides a 4.7 μm by 4.7 μm per pixel image resolution. A counter-propagating 632.8-nm beam from a HeNe laser focuses through the back of the sample by a cylindrical lens (f = 250 mm) to illuminate any damage pinpoints within the tested volume. To measure the damage

pinpoint sizes, the cw HeNe beam used to illuminate the damaged volume is replaced with a white light source. This is done to eliminate interference effects associated with monochromatic scattering (which exaggerates pinpoint damage site size and distorts morphology). The % 2 magnification microscope objective is replaced with a % 20 magnification microscope objective to provide 0.47 μm by 0.47 μm per pixel resolution. Greater detail regarding the damage testing system used in this work is described.[1]

The samples used in this work were cut to $1 \times 5 \times 5$ cm^3 size plates and polished on all sides. The KDP was grown using the rapid growth method and samples were doubler cut but the DKDP was conventionally grown and samples were tripler cut, each according to their use on the National Ignition Faciltiy (NIF). The plane containing the crystal axis was situated horizontally for each sample while the polarization of each harmonic beam was rotated to vertical when necessary in order to be perpendicular to the crystal axis.

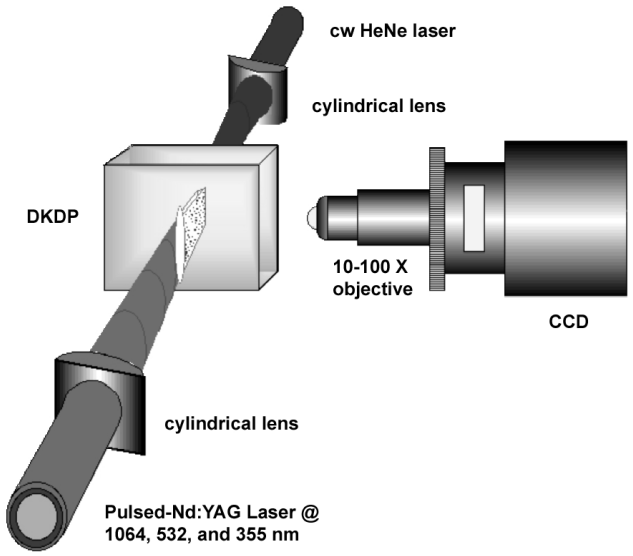

Figure 1. Experimental setup of damage performance testing system. A detailed description is provided in the text.

3. EXPERIMENTAL PROCEDURE

We devised methods to investigate the possibility that there are different defects leading to damage initiation at different wavelengths. We analyze the damage behavior of defects at the different wavelength harmonics as well as the individual damage site morphology. In the former case, the concept is described as follows: bulk sites previously damage tested at one wavelength are subsequently damage tested using another wavelength. The PPD resulting from each pulse can then be measured for comparison. With each pulse at a set fluence resulting in the same PPD N, a total PPD of 2N indicates two completely different populations. To realize this concept, we considered that the first pulse may condition the material and thus influence the PPD resulting from exposure to the second pulse. Ramp conditioning experiments were performed first to determine that neither 1064 nm nor 532 nm conditions for 355 nm, nor does 1064 nm condition for 532 nm. In the latter case, the morphology of damage sites at the individual wavelength harmonics under similar irradiation conditions is analyzed in order to provide further insight into nature of the defects leading to damage initiation.

3.1 Testing for multiple defect populations

First, the fluences for two different wavelengths for which damage testing of the pristine material will result in approximately the same PPD was determined. Ten pristine sites were then damage tested with single pulses for each of these two wavelengths, at the predetermined fluences. An image of each site was captured and the PPD was measured. The average PPD created at each wavelength was then calculated. We then returned to the first ten sites damage tested at

the first wavelength and damage tested over them at the second wavelength. Images of the damaged sites were then recaptured and the new PPD resulting from damage testing with the second pulse was determined. To measure the PPD, the number of pinpoints in the volume exposed to peak fluence (within 5%) is counted.

3.2 Damage site morphologies

Bulk volumes were damage tested with single pulses of the same fluence at each wavelength in order to observe any difference in the damage site morphologies with changes to only the wavelength to the pulse characteristics. White light scattering images of the damage sites were then captured at 90 degrees with respect to illumination using high resolution. Imaging software was used to maintain image contrast and the digitized intensity profiles in the horizontal and vertical dimensions of the images were calculated to show the amount of scatter from damage. Testing was performed using different fluences at each wavelength, however, comparison with low fluence at 1064 nm was not possible due to the high damage threshold at this wavelength and comparison with high fluence at 355 nm was not possible due to the onset of surface damage initiation.

4. EXPERIMENTAL RESULTS

4.1 Investigating the Different Types of Defects

Typical results are summarized in Table 1. Each PPD value represents the average PPD from the ten measurements and the standard deviation. Tables 1a and 1b show results for damage testing at 355 nm in material previously damage tested at 532 nm for different fluences at each wavelength (resulting in two different PPDs). Results for damage testing at 532 nm in material previously damage tested at 355 nm are also shown in Table 1c. Table 1d shows results for damage testing at 532 nm in material previously damage tested at 1064 nm. The left and middle columns show the average PPD at the two different wavelengths separately while the right column shows the results following damage testing with both wavelengths.

a)	DT @ 2ω, 19 J/cm^2	DT @ 3ω, 13.5 J/cm^2	DT @ 2ω, 19 J/cm^2 + 3ω, 13.5 J/cm^2
	111 ± 14 pp/mm^3	105 ± 17 pp/mm^3	129 ± 15 pp/mm^3
b)	DT @ 2ω, 16 J/cm^2	DT @ 3ω, 12.5 J/cm^2	DT @ 2ω, 16 J/cm^2 + 3ω, 12.5 J/cm^2
	57 ± 15 pp/mm^3	64 ± 11 pp/mm^3	68 ± 12 pp/mm^3
c)	DT @ 3ω, 13.5 J/cm^2	DT @ 2ω, 19 J/cm^2	DT @ 3ω, 13.5 J/cm^2 + 2ω, 19 J/cm^2
	105 ± 17 pp/mm^3	111 ± 14 pp/mm^3	116 ± 12 pp/mm^3
d)	DT @ 1ω, 41 J/cm^2	DT @ 2ω, 16 J/cm^2	DT @ 1ω, 41 J/cm^2 + 2ω, 16 J/cm^2
	59 ± 10 pp/mm^3	48 ± 15 pp/mm^3	105 ± 26 pp/mm^3

Table 1. The right column shows the results for damage testing at wavelength B (shown in middle column) in material previously damage tested at wavelength A (shown in left column) for a) A = 532 nm, B = 355 nm using fluences that result in ~ 110 pinpoints per mm^3, b) A = 532 nm, B = 355 nm using fluences that result in ~ 60 pinpoints per mm^3, c) A = 355 nm, B = 532 nm using fluences that result in ~ 110 pinpoints per mm^3, and d) A = 1064 nm, B = 532 nm using fluences that result in ~ 50 pinpoints per mm^3. Each box shows results for the average PPD and the standard deviation.

The top row (Table 1a) shows that damage testing pristine material at 19 J/cm^2 at 2ω resulted in 111 ± 14 pp/mm^3 and damage testing pristine material at 13.5 J/cm^2 at 3ω resulted in 105 ± 17 pp/mm^3. Damage testing at 13.5 J/cm^2 at 355 nm in the 532 nm tested sites resulted in a new total of 129 ± 15 pp/mm^3. The average total PPD resulting from damage testing at 532 nm followed by 355 nm is the same within experimental error as the average total PPD resulting from damage testing at 532 nm only. An example measurement of the averaged ten is shown in Figure 2. This experiment was repeated using various combinations of fluences and the results demonstrated the same behavior. For example, Table 1b shows a similar behavior when the PPD is about half to that discussed above. Pristine sites damage tested at 16 J/cm^2 at 532 nm resulted in 57 ± 15 pp/mm^3 and pristine sites damage tested at 12.5 J/cm^2 at 355 nm resulted in 64 ± 11 pp/mm^3. Damage testing at 12.5 J/cm^2 at 355 nm in the 532-nm tested sites results in a new total of 68 ± 12 pp/mm^3. Table 1c shows the experiment performed in reverse, that is the 532-nm followed by the 355-nm pulse. These experiments were also performed in order to confirm similar results despite the presence of some level of conditioning. The same fluences as those used in Table 1a were used but with each wavelength in reverse order. Damage testing at 19 J/cm^2 at 532 nm in the 355-nm tested sites resulted in a new total of 116 ± 12 pp/mm^3, the same PPD as the average total PPD resulting from damage testing at 355 nm only (105 ± 17 pp/mm^3) within experimental error. Table 1d shows that damage testing in pristine material at 41 J/cm^2 at 1064 nm results in 59 ± 10 pp/mm^3 and damage testing pristine material at 16 J/cm^2 at 532 nm resulted in 48 ± 15 pp/mm^3. Testing at 1064 nm followed by 532 nm resulted in a total PPD of 105 ± 26 pp/mm^3, equivalent to the added PPD resulting from the two wavelengths individually.

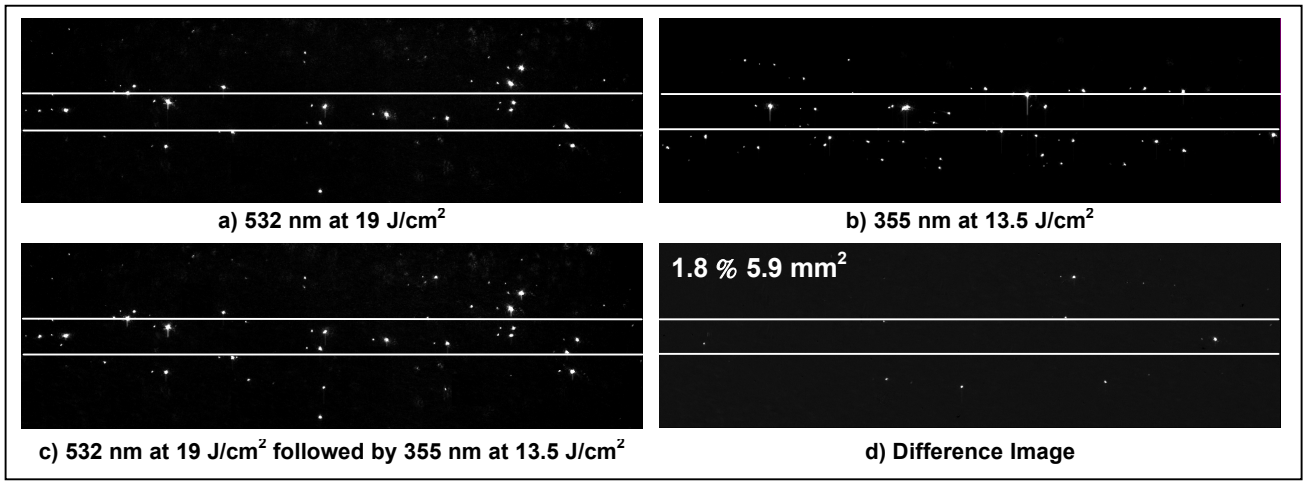

Figure 2. Results of damage testing at 355 nm in material previously damage tested at 532 nm. HeNe damage scatter images of a) ~ 100 pinpoints per mm^3 resulting from a single pulse at 19 J/cm^2 at 532 nm, b) ~ 92 pinpoints per mm^3 resulting from a single pulse at 13.5 J/cm^2 at 355 nm, c) ~ 111 pinpoints per mm^3 resulting from a single pulse at 19 J/cm^2 at 532 nm (shown in a)) followed by a single pulse at 13.5 J/cm^2 at 355 nm, and d) the difference image c) minus a) showing the new damage pinpoints from the 355-nm pulse.

4.2 Damage morphology different at 1064 nm

Figure 3 shows 100 % magnification white light scattering images of damage sites resulting from single pulses at each wavelength. The fluences of the pulses were ~ 46 J/cm^2 at 1064 nm (Figure 3a) and at 532 nm (Figure 3b) and ~ 20 J/cm^2 at 355 nm (Figure 3c) and at 532 nm (Figure 3d). Figure 4 shows the digitized intensity profiles along horizontal and vertical directions in the 1064- and 532-nm damage images (Figures 3a and 3b, respectively) indicated by the white dashed arrows. Figures 4a and 4b shows the intensity profiles for the 1064- and 532-nm damage, respectively.

Images of the damage sites resulting from irradiation at 1064 nm (Figure 3a) suggest the presence of a core that strongly scatters light surrounded by much a larger volume containing a network of cracks. The image intensity profile along a vertical direction passing near the cores of several damage site (indicated by a dashed line in Figure 3a) is shown in Figure 4a. This profile reveals the presence of significant scattering in the material volume containing the surrounding

cracks. The intensity profile taken along a horizontal direction was chosen to intersect two damage site cores (see Figure 3a). As a result, the peaks in the intensity profile are due to scattering by the core of the damage sites. Near these peaks, the observed scattering is due to cracks surrounding the larger core. The diameters of the cores were estimated from the FWHM of the intensity profile of the image and were found to be in the range of 15-45 μm. The surrounding network of cracks extends farther resulting in the observation of scattering from each damage site ranging 100-300 μm across.

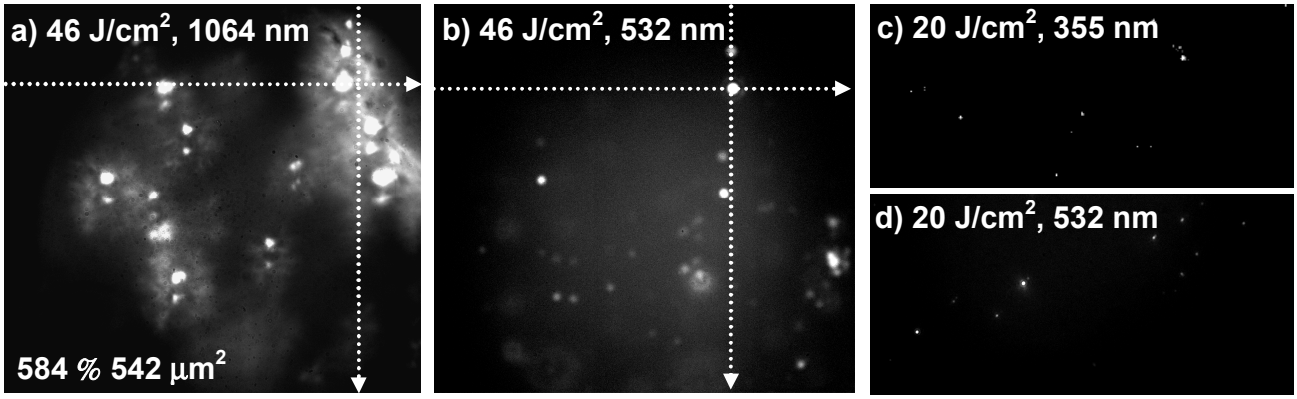

Figure 3. 20 % white light scattering images of damage sites resulting from a single pulse at a) 1064 nm at 46 J/cm^2, b) 532 nm at 46 J/cm^2, and c) 355 nm at 20 J/cm^2. Damage site cores have dimensions of 15-45 μm in diameter with the damage from 1064 nm while dimensions of 3-5 mm are observed with 532 and 355 nm.

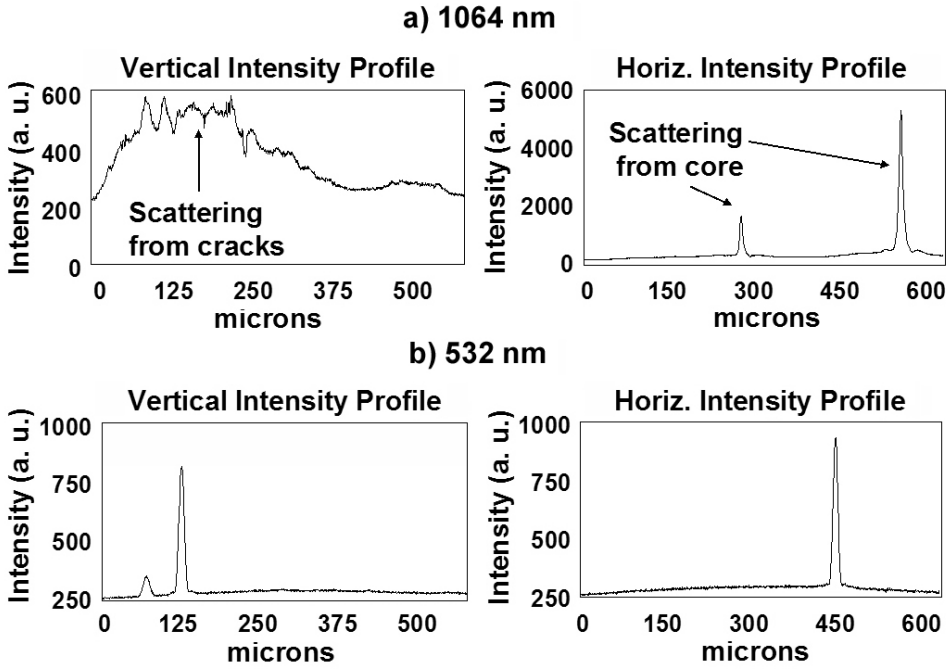

Figure 4. Digitized scattering intensity profiles along horizontal and vertical directions of damage sites resulting from a) 1064 nm and b) 532 nm (shown as white dashed arrows in Figures 1a and 1b). Scattering from cracks are visible with damage sites from 1064 nm and not with damage sites at 532 nm.

Damage sites resulting from 532-nm irradiation are shown in Figure 3b. These sites exhibit scattering from damage cores but there is no evidence indicating the presence of a crack network such as that seen in damage sites formed under

1064-nm irradiation. Both the vertical- and horizontal-direction intensity profiles shown in Figure 4b are taken along directions that intersect damage site cores. The vertical-direction intensity profile is also taken along a direction near to several damage site cores but no scattering above background is observed that can be attributed to the formation of cracks. The FWHM of the scattering intensity profiles of the images indicate that the size of the cores range from 15-45 μm in diameter.

Figures 3c and 3d show damage sites from single pulses at about 20 J/cm^2 at 355 and 532 nm, respectively. The images indicate that the size of the cores is ranging between 3-5 μm for both wavelengths. This indicates that the size of the diameter of the core increases with increasing laser fluence. Overall, damage sites resulting from each wavelength consistently have the same core sizes for the same fluences but with cracks only surrounding many of the 1064-nm damage sites. We also observed in the samples we investigated that although the damage sites resulting from 532- and 355-nm irradiation are evenly distributed within the bulk of the material (at least within small volumes), the damage sites resulting from 1064-nm irradiation appears to be concentrated in certain region with an interconnected network of crack to form clusters of damage sites.

5. DISCUSSION

The results of the damage testing experiments to investigate the defect populations involved indicate the presence of two distinct populations. More specifically, in the case of testing at 355 nm following 532 nm, there remains a total PPD equivalent to that resulting from the first of the two pulses irradiated at each wavelength. These results strongly suggest that there is at least a large overlap in the defects leading to damage initiation at 532 nm with those at 355 nm. Moreover, these results were consistent when repeated using different fluence levels (resulting in different PPDs at each wavelength). This further indicates that the defects at 532 and 355 nm initiate damage in the same sequence (with increasing fluence). In contrast, in the case of testing at 355 or 532 nm following testing at 1064 nm, there is an observed total PPD equivalent to the addition of damage from each wavelength separately. This indicates that there is at least a large non-overlap of the defects leading to damage initiation at 355 and 532 nm with those leading to damage initiation at 1064 nm.

Under similar irradiation conditions and imaging contrast, damage sites at all three wavelengths have cores of the same size (3-5 μm for damage initiated at ~ 20 J/cm^2 and 15-45 μm for damage initiated at ~46 J/cm^2). The damage sites resulting from 1064-nm exposure are often surrounded by a network of cracks extending for hundreds of microns. The dissimilarities in the morphologies of damage sites at 1064 nm are consistent with the presence a different type of defects responsible for damage initiation at 1064 nm than at both 355 and 532 nm. In work by Runkel et al., thermal annealing of KDP crystals has also been shown to increase the damage performance at 1064 nm and not at 355 nm[1] further suggesting the presence of a different type of defects responsible for damage initiation at 1064 nm. Other work presented in this proceedings that investigates the damage behavior under simultaneous exposure to 355- and 532-nm irradiation which also indicates the presence of one type of defects leading to damage initiation at both wavelengths and, moreover, that these defects initiate damage in the same sequence independent of the wavelength.

ACKNOWLEDGEMENTS

This work was performed under the auspices of the U.S. Department of Energy by University of California, Lawrence Livermore National Laboratory under contract W-7405-Eng-48.

REFERENCES

1. P. DeMange, C. W. Carr, H. B. Radousky, and S. G. Demos, "System for evaluation of laser-induced damage performance of optical materials for large aperture lasers," *Rev. Sci. Instrum*. **75**, 3298 (2004).
2. M. J. Runkel, S. M Maricle, R. Torres, J. Auerbach, R. Floyd, R. Hawley-Fedder, and A. K. Burnham, "Effect of thermal annealing and second harmonic generation on bulk damage performance of rapid-growth KDP type I doublers at 1064 nm," in *Laser-Induced Damage in Optical Materials: 2000*, Gregory J. Exarhos, Arthur H. Guenther, Mark R. Kozlowski, Keith L. Lewis, M. J. Soileau, Eds., *Proc. SPIE* **4347**, 389-399, 2001.

3. R. A. Negres, P. DeMange, H. B. Radousky, S. G. Demos, “Laser-Induced Damage in DKDP Crystals under Simultaneous Exposure to Laser Harmonics,” in these proceedings **5991-30**.